Oil Shale, 2024, Vol. 41, No. 4, pp. 289–308
doi: https://doi.org/10.3176/oil.2024.4.04
ISSN 0208-189X

Effect of air staging on low-NO_x combustion performance of regenerative heating furnace for oil shale retort

Yue Yue[(a,b)]*, Zhu He[(a)], Chunhua Wang[(b)]*

[(a)] Department of Materials, Wuhan University of Science and Technology, Wuhan 430065, China
[(b)] College of Petroleum Engineering, Liaoning Petrochemical University, Fushun 113001, China

Received 26 May 2024, accepted 18 October 2024, available online 31 October 2024

Abstract. *A top-fired heating furnace is a type of heating equipment for the heat carrier used in the dry retorting process of oil shale. This study explores the energy consumption and pollutant emissions of such furnaces, focusing on the influence of the excess air coefficient and air staging ratio on the NO emission characteristics of the combustion chamber outlet, using the numerical simulation method. The research shows that with the increase of the excess air coefficient α, the combustion chamber temperature and the NO emission value of the combustion chamber outlet first increase and then decrease, reaching a peak at α = 1.05. The combustion chamber temperature directly affects the NO emission value, showing the change law of thermodynamic NO with temperature. When the air is staged, the factors affecting the NO emission value are more complicated, and the amount of NO generation is not only affected by the uniformity of combustion temperature but also by the mixing characteristics. When the proportion of secondary air is 30%, the mixing fraction distribution is the most uniform, the mixing effect of fuel gas and air is the best, and the NO emission value at the combustion chamber outlet is the lowest.*

Keywords: *top-fired heating furnace, oil shale retort, excess air coefficient, air staging combustion.*

1. Introduction

Oil shale is an unconventional energy resource with rich reserves, exceeding coal reserves by nearly 40%. Oil shale is usually used as a raw material for the production of shale oil. Typically, oil shale is mined, crushed, screened,

* Corresponding authors, yueyue92976@163.com, wangchunhua@lnpu.edu.cn

and processed in a retort to produce shale oil [1]. A crucial component in the low-temperature retorting process is the reheating furnace, commonly of a regenerative type, which provides the high-temperature heat carrier for shale retorting.

The top-fired heating furnace is a specific type of furnace for oil shale retorting. As shown in Figure 1, the most significant feature is that the combustion chamber is located in the upper part, and the top is provided with a circular mixing chamber, so that fuel gas and air are mixed through continuous rotation and cutting, ensuring complete mixing and also enabling the mixed gas to be ejected at a certain speed and direction to achieve complete combustion. The symmetrical structure of the furnace further ensures an evenly distributed flow field, allowing for a 15 to 20% increase in the heat storage area with the same furnace capacity, greatly improving thermal efficiency [2]. The fuel gas used in this process is the combustible waste gas produced by oil shale retorting. Due to the gasification of semi-coke by air through the Fushun distillation process, a large amount of nitrogen is mixed, resulting in a very low calorific value of the gas, generally around 4000 kJ/m^3 [3], classifying it as low calorific value gas.

However, as the global air pollution problem becomes more serious, air quality continues to deteriorate, leading to increasingly stringent emission restrictions on pollutants, especially for nitrogen oxides (NO_x), which cause substantial environmental harm. To overcome this challenge, the conventional top-fired furnace combustion process must adhere to stricter NO_x emission standards. At present, NO_x emissions exceed the limits set by China's national emission standards ($\leq$100 mg/m^3 [4–6], converted to 3.6% O_2 concentration). Moreover, NO_x is highly harmful to human health, with known carcinogenic effects [7]. Therefore, achieving efficient combustion of low-calorific gas while minimizing pollutant emissions has become an urgent problem to be solved.

Factors influencing NO_x formation include combustion temperature and its uniformity [8, 9], excess air coefficient [10], and oxygen content [11]. Therefore, maintaining optimal temperature distribution, air volume, and oxygen content in the combustion zone forms the core of low-NO_x combustion technology, designed to prevent NO_x generation and minimize emissions. This technology must ensure stable furnace combustion and keep the carbon monoxide (CO) content in the flue gas within regulatory standards.

Presently, major low-NO_x combustion technologies include air-staged combustion [12, 13], fuel-staged combustion [14, 15], fully premixed combustion [16], and flue gas recirculation [9, 10, 17]. Among these, air-staged combustion technology is particularly effective and economical. The combustion intensity is adjusted by introducing air in multiple stages. Initially, a rich-fuel combustion is created, forming a reducing atmosphere that converts some of the NO_x into N_2, thereby inhibiting further NO_x formation. In addition, staged combustion induces lower fuel combustion speed and temperature

compared to uncontrolled combustion methods, further limiting thermal NO_x emissions. The final stage culminates in full fuel combustion.

Many scholars have studied air-staged combustion technology and achieved good results. Pan [12] developed a new low-NO_x multi-stage air burner and established its numerical model. By calculation, the optimum ratio of primary, secondary, and tertiary air in natural gas burners is determined to be 21.68%, reducing NO_x emissions in the flue gas to 53 mg/m^3 (converted to 8% O_2 concentration). Wang et al. [18] analyzed the airflow dynamics within an air-staged combustion system using numerical simulation and found that air staging increases the residence time of small solid particles, while making the furnace temperature more uniform. Li et al. [19] conducted an experiment on controlling NO_x emissions using air-staged combustion in small- and medium-sized biomass boilers. They introduced innovative designs for the secondary air inlet pipe and fuel pipe, and determined the staged-air ratio and excess air coefficient suitable for these boilers. These research results provide theoretical and numerical simulations for the design and optimization of low-NO_x burners, exploring the utility and performance of air-staged combustion technology.

The top-fired heating furnace operates through diffusion combustion, where fuel and oxidizer collide and rise from each nozzle, creating a high-velocity vertical flow loop. This circulation zone forms due to the sudden expansion of the wall surface of the combustion chamber, with the main turning zone located towards the bottom, concentrated in the center of the chamber. There is also a diversionary flow swirling upwards, impacting the arch wall before folding back and creating a minor loop area at the top of the chamber. Under this flow field, the combustion temperature gradually rises, resulting in the appearance of a local high-temperature phenomenon. Moreover, the asymmetrical flow pattern within the furnace increases the likelihood of local high-temperature occurrence, resulting in significant NO_x production.

To solve this problem, we need to improve the mixing mode of fuel and air, achieve rapid mixing, and make the temperature as uniform as possible. One potential method is to implement staged combustion by spraying combustion-supporting air at the top, while maintaining the existing burner (pre-combustion chamber) structure. The staged combustion mode consists of two phases: anoxic combustion and oxygen-enriched combustion. In the first phase, gas and air undergo anoxic combustion, followed by oxygen-enriched combustion in the second phase. By spraying combustion air at the top, the temperature of the pre-combustion chamber is easily adjustable. However, the temperature profile and emission characteristics in the combustion chamber become more complex after upgrading. Therefore, computational fluid dynamics analysis is employed to explore the temperature field, flow field, and NO_x emission behavior in the top-fired heating furnace with a top air jet structure, aiming to improve the problems of insufficient mixing, uneven temperature distribution, and excessive NO_x emissions.

2. Research object

The top-fired heating furnace used for oil shale distillation is cylindrical with a semi-spherical top. The overall structure consists of four parts: the pre-combustion chamber, combustion chamber, regenerator chamber, and grate. The lower part of the pre-combustion chamber connects to the combustion chamber, where the fuel and combustion air emitted by the nozzle are burned. The regenerator is made of lattice bricks arranged into stacks. These lattice bricks contain many vertical grid holes. The brick grates are supported by iron grates and pillars beneath them.

The furnace realizes the cyclical operation of the combustion and heating periods. During combustion, high-temperature flue gas is produced from fuel combustion in the combustion chamber, flowing through the lattice bricks in the regenerator chamber to heat them to a high temperature. The bricks temporarily store the heat of the flue gas, while the cooled flue gas is discharged from the exhaust port at the bottom of the furnace.

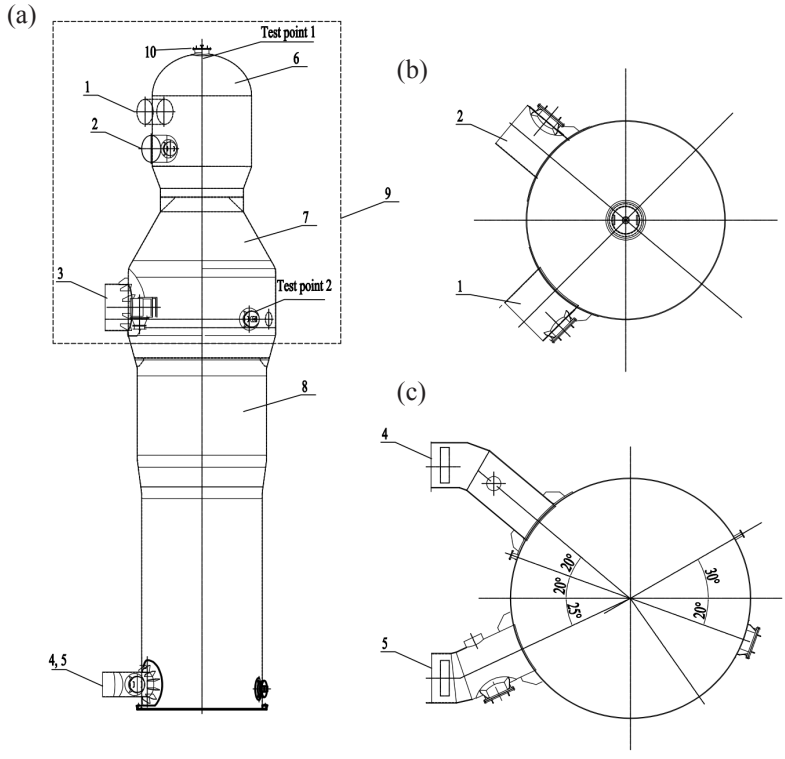

Fig. 1. Structure diagram of the top-fired heating furnace: main structure of the heating furnace (a), fuel gas nozzle and air nozzle structure (b), bottom flue gas outlet and cold cycle gas inlet (c). 1 – fuel inlet, 2 – primary air inlet, 3 – hot cycle gas outlet, 4 – flue gas outlet, 5 – cold cycle gas inlet, 6 – pre-combustion chamber, 7 – combustion chamber, 8 – regenerator chamber, 9 – research area, 10 – secondary air inlet.

During the heating period, cold cycle gas enters the regenerator, absorbs heat from the high-temperature bricks, and is converted into hot cycle gas, which then becomes a qualified hot carrier gas for subsequent retort furnaces. After certain heating time, the heat stored in the furnace decreases, and the cold cycle gas can no longer be heated to the required temperature. At this point, the process shifts from the heating period back to the combustion period.

The combustion and heating periods alternate in sequence. In this continuous two-period cycle, three heating furnaces are usually built and arranged in sequence within the industry, with two furnaces operating in the combustion period and the third one in the heating period [20].

NO_x emissions and reductions primarily occur in the furnace's combustion chamber. For greater focus and faster computation, we selected the pre-combustion chamber and combustion chamber, as shown within the dashed boundary of Figure 1. The overall height of the furnace is 29,700 mm, including a pre-combustion chamber of 6400 mm and a combustion chamber of 7247 mm in height. The inner diameters of the pre-combustion and combustion chambers are 4484 and 6640 mm, respectively. Four layers of nozzles were installed: the top two layers are fuel gas nozzles, arranged in a cross pattern with 12 nozzles per layer, totaling 24 nozzles. The lower two layers are air nozzles, also arranged crosswise, with a total of 24 nozzles. The vertical inclination angle of the upper nozzle was set at 19°.

3. Numerical simulation

The numerical simulation was conducted with numerical computational fluid dynamics software, using the mass, energy, momentum, and composition conservation equations of the steady-state reaction flow, as well as achievable k-ε turbulence models, non-premixed combustion models, discrete ordinates radiation models, and NO_x models, as shown in reference [21]. In this study, gas combustion-derived NO_x encompasses solely thermal/fast NO_x, excluding fuel NO_x. Notably, the primary NO_x constituent of gas combustion is NO, so the focus here is on NO emissions.

3.1. Grid division and boundary conditions

Figure 2 shows the grid division of the study objects. The calculation area adopted a hybrid grid. The pre-combustion chamber of the heating furnace, which connects the gas nozzle and the air nozzle, has a complex structure and is therefore meshed with tetrahedral elements and locally refined. Other areas use hexahedral grids. Based on mesh independence analysis, the total amount of mesh in the final calculation area was about 3 million.

The fuel used was the exhaust gas produced during the oil shale retorting process, with its composition shown in Table 1. The boundary conditions at the gas nozzle and the air nozzle adopted the velocity inlet, and the air ejection

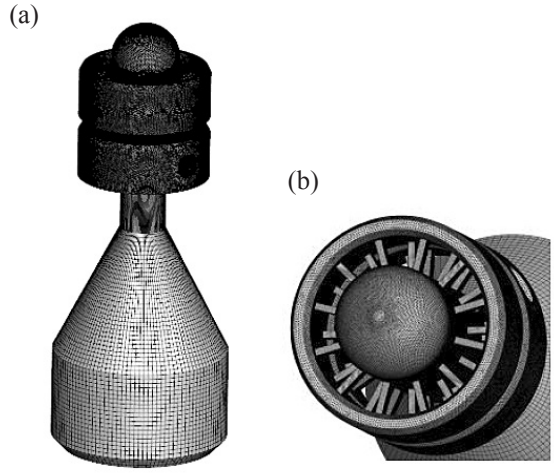

Fig. 2. Grid division: overall calculation area (a) and partial amplification at the nozzle (b).

velocity was calculated based on the excess air coefficient. The connecting section between the combustion chamber and the regenerator chamber was regarded as the flue gas outlet, and the boundary was set as the pressure outlet. The specific values for each boundary condition are shown in Table 2.

Table 1. Fuel gas composition

Component, %vol	CH_4	H_2	C_2H_4	CO	CO_2	N_2
	6.0	11.0	1.0	4.0	20.4	57.6

Table 2. Boundary conditions

Cases	Fuel inlet			Air inlet		
	Velocity, m/s	Temperature, K	Equivalent diameter, mm	Velocity, m/s	Temperature, K	Equivalent diameter, mm
Values	8.38	324.15	581	Calculated based on the excess air coefficient	274.15	693

3.2. Verification of the numerical simulation method

To validate the accuracy of the adopted numerical simulation method, two top-fired heating furnaces, labeled 1 and 2, which are currently in operation on-site, were selected for practical testing.

First, two key test points were set up inside the furnaces: one in the dome and the other in the combustion chamber. As shown in Figure 1, test point 1 was located in the dome, 28.19 m from the furnace bottom, and mainly monitored temperature variations at the dome. Test point 2, situated in the combustion chamber, was 17.11 m from the furnace bottom and was used to monitor temperature changes within the chamber. These test points provided essential information about the temperature distribution inside the furnace. The test results are shown in Tables 3 and 4.

Next, a detailed numerical simulation was carried out for the operating conditions of furnaces 1 and 2. This included modeling the combustion process, heat transfer, fluid flow, and other physical phenomena inside the furnaces. The models and parameters used in these numerical calculations were based on the actual operating conditions and design parameters of the furnaces.

After completing the numerical calculations, the calculated temperatures at the corresponding positions of test points 1 and 2 were compared with the actual test data. In addition, NO emission levels at the furnace outlet were compared, as these were important indicators for evaluating combustion efficiency and environmental performance.

Table 3. Operating parameters of the heating furnaces

No.	Air parameter			Fuel parameter		
	Temperature, K	Pressure, Pa	Volume flow rate, Nm^3/h	Temperature, K	Pressure, Pa	Volume flow rate, Nm^3/h
1	274.15	6800	6379	324.15	9800	7393
2	273.75	6900	6379	322.15	9800	7393

Table 4. Comparison of numerical simulation and experimental data

Air temperature, K	Data status	Temperature, K		NO emission value at the furnace outlet, mg/Nm^3
		Test point 1	Test point 2	
274.15	Measured data	618	1146	27
	Simulation data	656	1199	28
	Error	6.1%	4.6%	3.7%
273.75	Measured data	621	1145	43
	Simulation data	588	1203	45.8
	Error	–5.3%	5.1%	6.5%

4. Results and discussion

4.1. Effect of the excess air coefficient

While keeping other parameters unchanged, the excess air coefficient α was changed from 0.78 to 1.1 to explore its specific influence on the combustion characteristics and NO emission characteristics of the combustion chamber.

Figures 3–5 show the streamline distribution, mixing fraction distribution, and temperature distribution for different α values in the Z = 0 surface. The fuel enters the furnace, and due to the widening of the passage and the extrusion of the opposite airflow, part of the fuel flows to the dome area, touches the arch wall, and returns, forming a small reflux area near the dome wall. Another part of the fuel flows directly to the combustion chamber outlet and meets the airflow (Fig. 3). Under the throat, due to the sudden expansion of the combustion chamber, two large areas of reflux are formed, which are mostly symmetrical. With the increase of α, the width of the left circumflex area in the center and the return area in the upper part of the combustion chamber also increase. However, the right rotation zone in the middle of the combustion chamber gradually decreases, resulting in the smallest and asymmetrical return zone in the middle of the combustion chamber when α = 1.05. This indicates that the mixing effect of fuel and combustion air in the combustion chamber is the worst under this condition.

The mixture of fuel and air can be represented by the mixture fraction (Fig. 4). When fuel and air are burned in chemical equivalence, the mixture fraction is 0.52, and α = 1, forming a flame at a higher temperature. When the local mixture fraction is greater than 0.52, the region is fuel-rich, and when less than 0.52, it is fuel-poor. Above the throat, the mixture fraction is generally greater than 0.52, indicating a fuel-rich zone where fuel and air gradually mix,

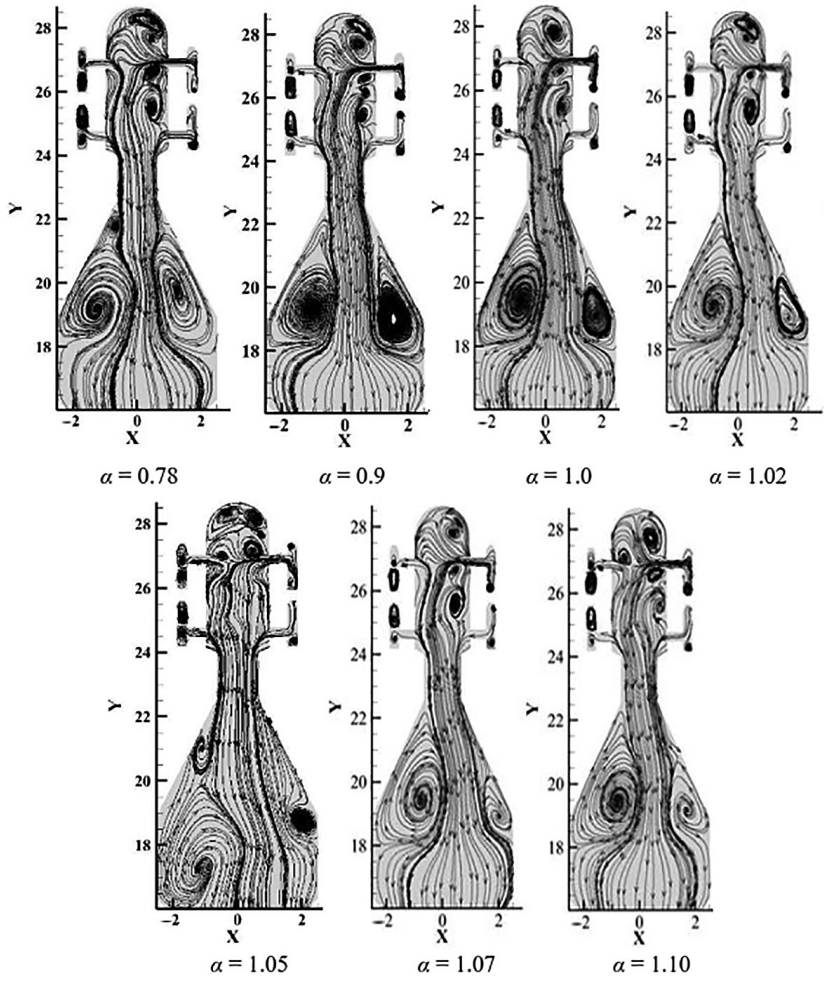

Fig. 3. Streamline distribution at different excess air coefficients α (Z = 0 surface).

leading to a slow chemical reaction and low combustion temperature (Fig. 5). As the mixed airflow moves downward into the reduced section of the throat, the mixing of fuel and air intensifies. Below the throat, the mixture fraction gradually approaches 0.52, allowing chemical equivalence combustion to occur.

Increasing α raises the oxygen concentration while reducing the flame temperature. From the general trend, with the increase of α, the combustion temperature and NO production first rise, reaching an extreme value, and then decrease. In premixed combustion, when $\alpha = 1$, the combustion temperature and NO production peak. However, in diffusion combustion, fuel and air mix and burn side by side; when $\alpha = 1$, fuel and air cannot mix evenly, preventing

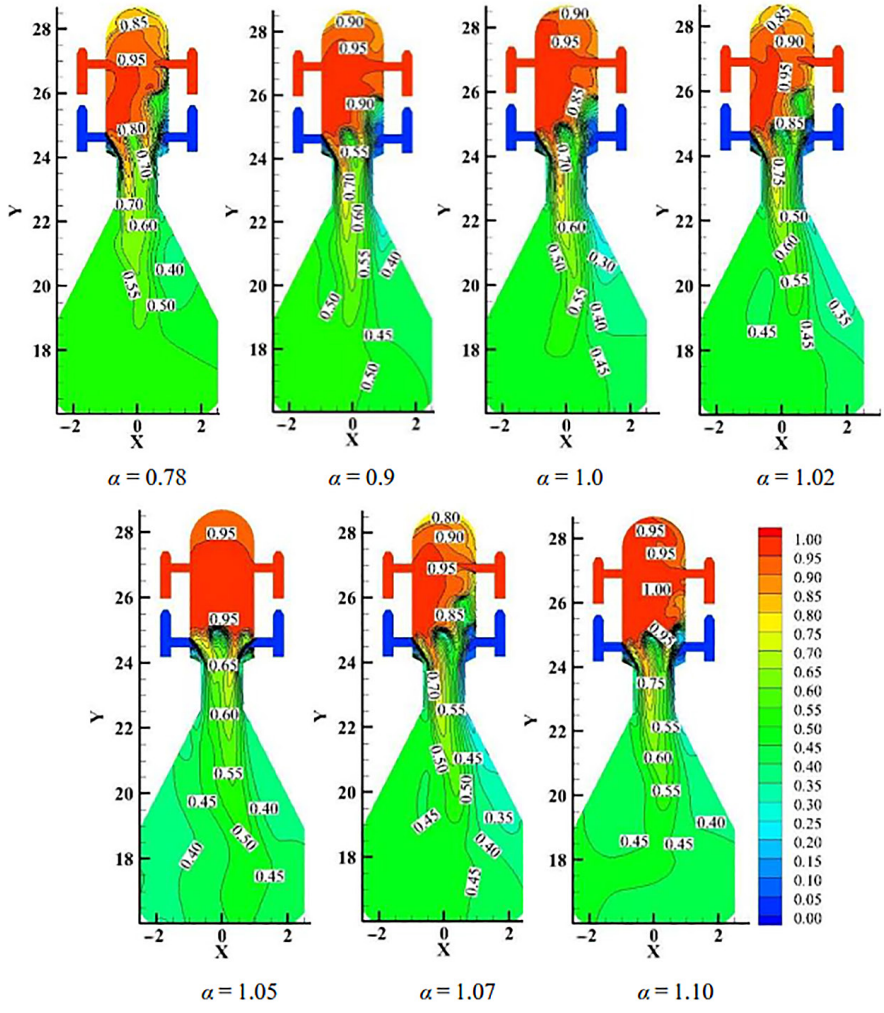

Fig. 4. Mixing fraction distribution at different excess air coefficients α (Z = 0 surface). The color figure is available in the online version of this journal.

chemical equivalence combustion. With the increase of α, the position of chemical equivalence combustion moves downward, the combustion temperature gradually rises, the high-temperature zone gradually expands, and NO emission levels gradually increase until α = 1.05. Then, further increases in α cause the combustion temperature, high-temperature zone, and NO emission levels to decrease gradually.

This is consistent with the findings of other studies. Zeng [22] and Chen et al. [8] found in gas combustion tests that the maximum flame temperature first increased and then decreased, with the transition range between 1.0 and 1.2. It can be seen in Figure 6 that the change of NO emission concentration at the outlet of the furnace is similar to the change trend of the maximum

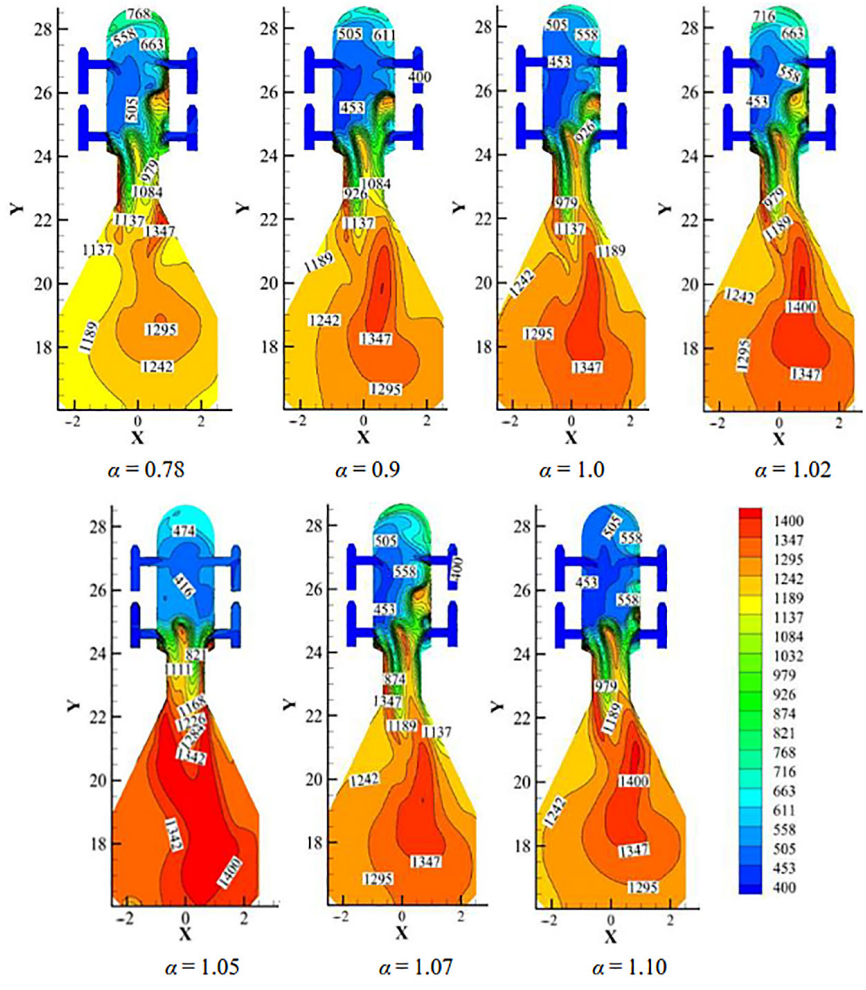

Fig. 5. Temperature distribution at different excess air coefficients α (Z = 0 surface). The color figure is available in the online version of this journal.

and average combustion temperatures in the furnace. With the increase of α, the maximum furnace temperature, average furnace temperature, and NO emission concentration at the furnace outlet all initially rise, peaking at α = 1.05, and then decrease. This is consistent with the law that the thermal NO production varies with temperature.

4.2. Effect of staged-air ratio

Air-staged combustion technology involves directing some air into the primary combustion zone, forming a fuel-rich environment with lower oxygen levels. This helps reduce NO emissions. Additional air is then added as secondary or tertiary air, ensuring that fuel is burned efficiently and reducing overall

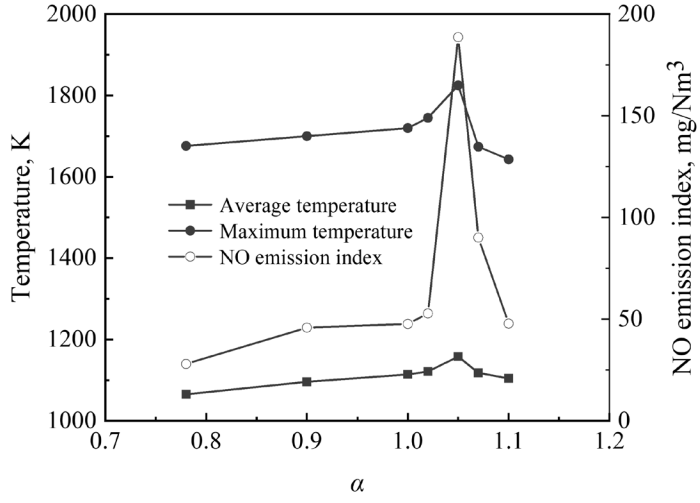

Fig. 6. Relationship between furnace temperature and NO emission concentration at the furnace outlet at different excess air coefficients α.

NO_x emissions. However, an imbalance in the staged-air ratio could lead to increased NO emissions. Our research showed that at $\alpha = 1.05$, NO emissions from the combustion chamber outlet peaked at 189 mg/Nm^3. Here, we focused on the impact of air staging on these emissions. Primary air was introduced through the original air nozzle, while secondary air was supplied through the dome nozzle. We defined r as the ratio of secondary air volume to total air volume, adjusted the value of r, and observed the specific effects of staged-air supply on combustion characteristics and NO emission characteristics of the heating furnace.

4.2.1. Analysis of the flow field in the combustion chamber

Figure 7 illustrates the velocity streamline within the combustion chamber (Z = 0 surface) under different secondary air ratios r. Notably, a reverse flow zone appears near the dome, the gas nozzle, and below the combustion chamber. As we increased the ratio r, the incoming velocity of the secondary air gradually escalated, thus increasing the momentum of the airflow entering the combustion chamber, while maintaining a stable vortex structure of the reverse flow zone on both sides of the jet center. However, when $r > 30\%$, the vortex structure of the reverse flow zone underwent significant deterioration. In the lower part of the combustion chamber, two vortices are fed by the blended airflow entering from the throat into the progressively enlarged combustion chamber. As we raised the ratio r, the two vortices gradually expanded, creating a comprehensive and symmetrical reverse flow zone vortex when $r = 30\%$. Subsequently, as r increased, the area of the reverse flow zone

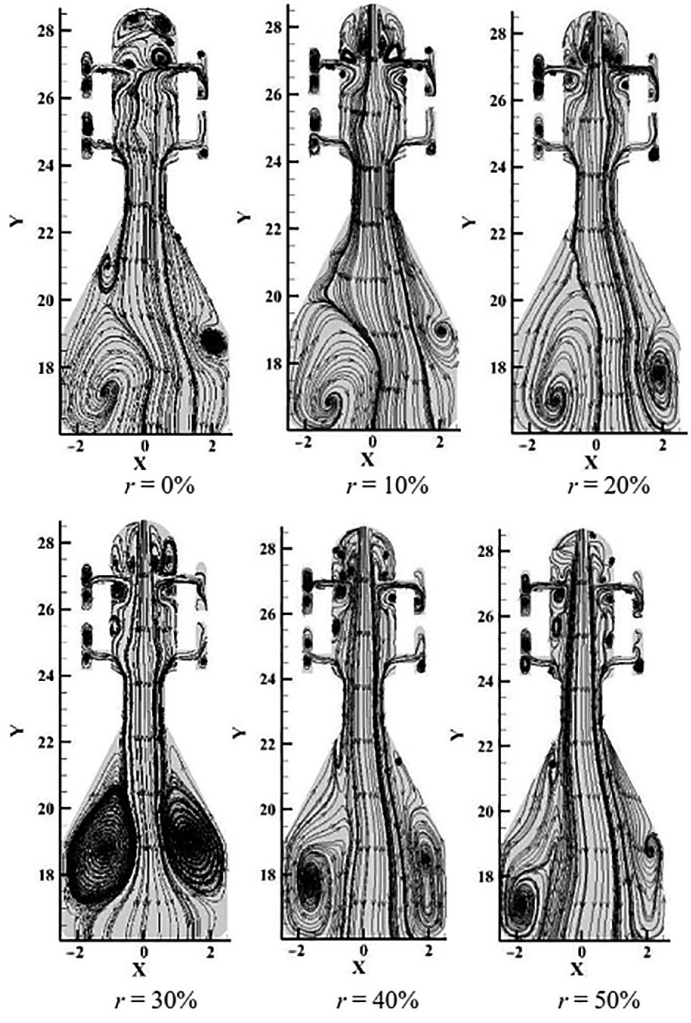

Fig. 7. Streamline distribution at different secondary air ratios *r* (Z = 0 surface).

decreased and became increasingly asymmetrical. This indicates that *r* = 30% exerts an optimal flame stabilization effect.

Figure 8 illustrates the mixing fraction of the combustion chamber (Z = 0 surface) under different air classifications. As *r* was raised, the incorporation of secondary air into the ambient fluid increased, enhancing the mixing of secondary air and the fuel flow. At *r* = 30%, optimum homogeneous mixing was achieved at the throat outlet, and the mixing fraction approached the mixing fraction corresponding to chemical equivalence combustion. In the combustion chamber, this supply air ratio also exhibited a relatively uniform mixing fraction. It shows that under this working condition, the mixing effect of fuel and air exceeds that of other supply air ratios.

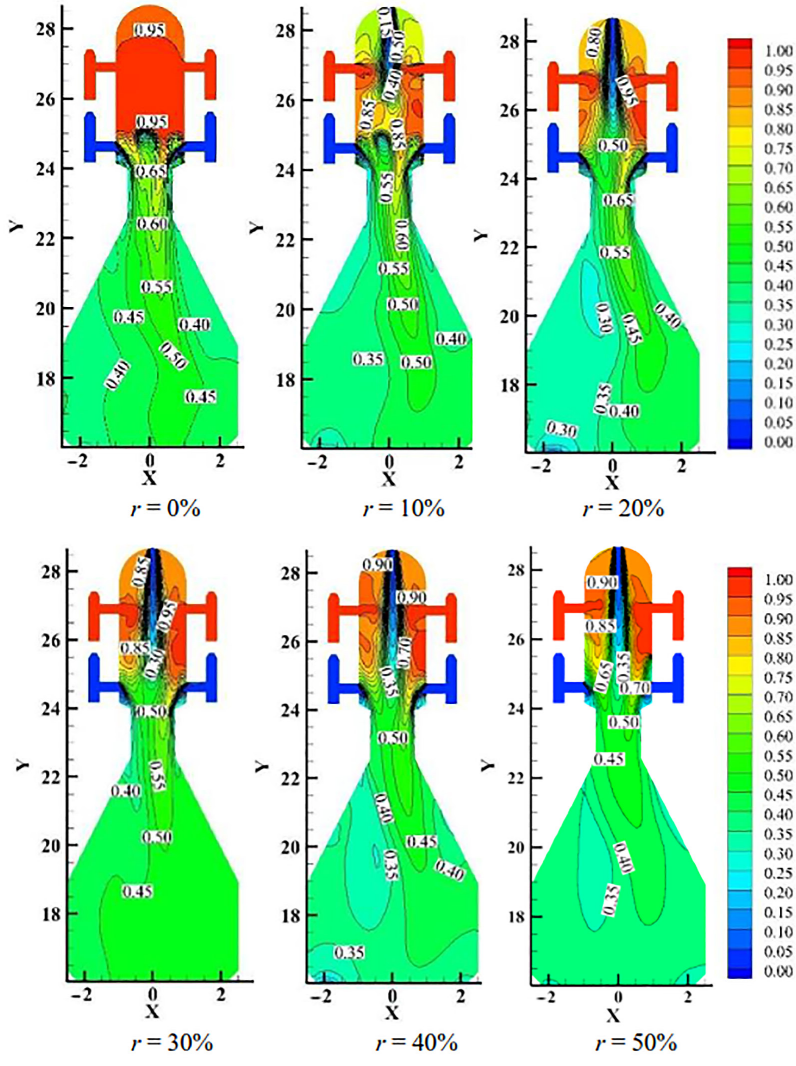

Fig. 8. Mixing fraction distribution at different secondary air ratios *r* (Z = 0 surface). The color figure is available in the online version of this journal.

4.2.2. Analysis of the temperature field in the combustion chamber

Figure 9 illustrates the temperature distribution within the combustion chamber (Z = 0 surface) under different air classifications. As depicted, the high-temperature zone is primarily distributed at the throat of the combustion chamber and below the throat, indicating that combustion mainly occurs in these two areas. As the ratio *r* increases, the starting point of the high-temperature zone shifts closer to the throat, indicating that an increase in the secondary air ratio *r* and a decrease in primary air promotes rapid fuel

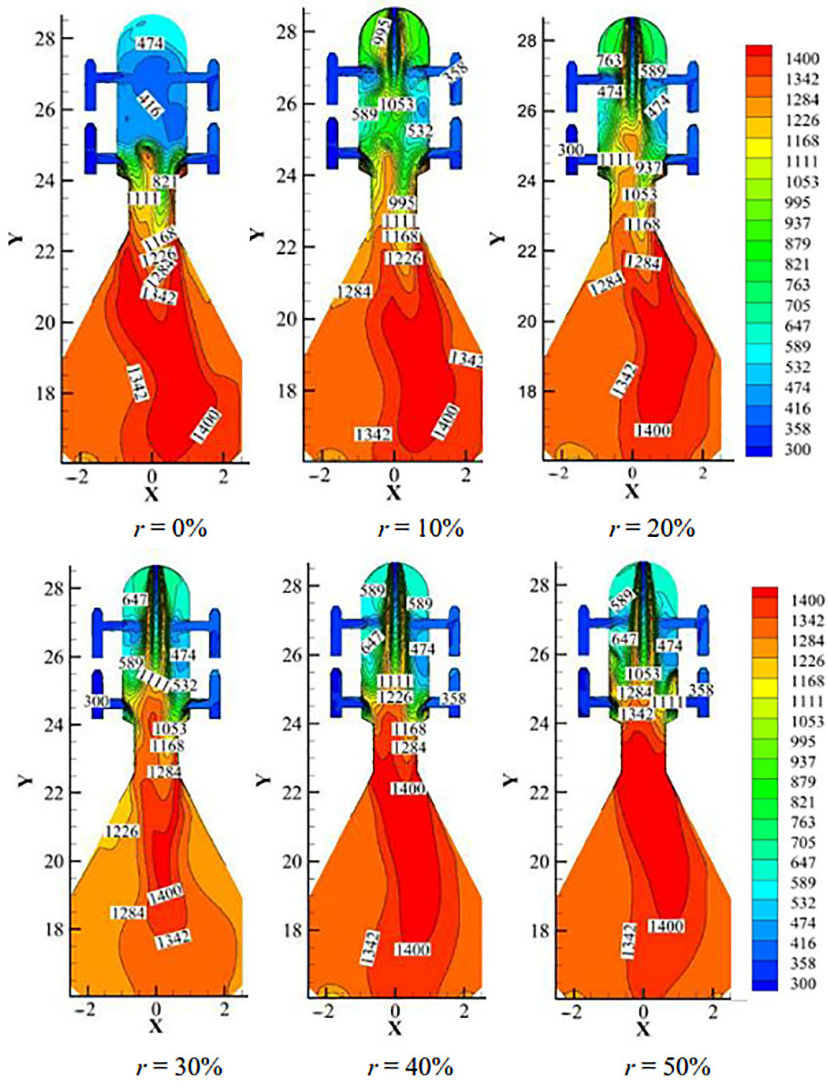

Fig. 9. Temperature distribution at different secondary air ratios *r* (Z = 0 surface). The color figure is available in the online version of this journal.

and air mixing and combustion. When *r* = 30%, as shown in Figure 9, the mixing effect of fuel and air is the best, and the resulting flame is the shortest, indicating that fuel and air achieve rapid and efficient combustion. The flame length is longer under other working conditions.

4.2.3. Analysis of factors influencing NO emission levels

As illustrated in Figure 10, the thermal variation within the combustion chamber does not have an identical impact on the NO emission levels at the combustion

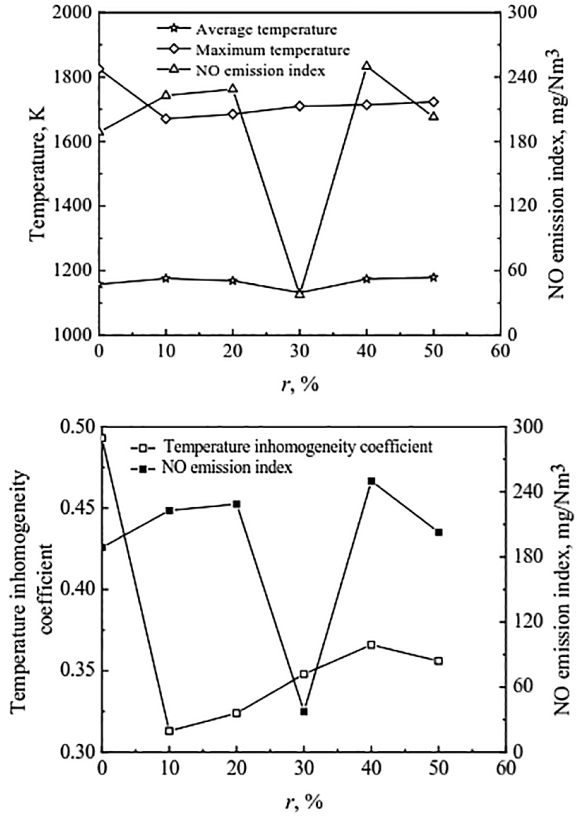

Fig. 10. Relationship between NO emission levels, furnace temperature, and temperature inhomogeneity coefficient at different secondary air ratios *r*.

chamber outlet. This revelation suggests that altering the air classification ratio amplifies the complexity of the elements influencing NO generation, significantly surpassing mere alteration in combustion temperature.

To further investigate whether the inhomogeneity of the temperature field has a significant impact on NO generation in the staged-air condition, an inhomogeneity coefficient of the temperature field was introduced, and its value was calculated using the following formula [23]:

$$x = \frac{\sqrt{\frac{1}{m}\sum_{j=1}^{m}(T_{ij} - \overline{T})^2}}{\overline{T}}, \tag{1}$$

where T_{ij} denotes the temperature value at point j within the combustion chamber under case i, $\overline{T}$ represents the average temperature within the combustion chamber under case i, and x signifies the temperature inhomogeneity coefficient, with lower values indicating a more uniform temperature field.

Taking the Z = 0 surface as an example, the temperature field for this section was calculated. The results are plotted in the right graph of Figure 10. These findings indicate that variations in the temperature uniformity of the combustion chamber do not dictate the specific magnitude of NO emission levels at the combustion chamber outlet. This shows that NO production is correlated not only with combustion temperature and uniformity, but also interconnected with other factors.

In the complex chemical reaction process of diffusion combustion, NO yield is also associated with mixing characteristics. As demonstrated in Figure 8, when the proportion of secondary air reaches 30%, the mixture fraction distribution is most consistent, with the mixing fraction approaching 0.52, being superior to other cases. This indicates that the excess air volume across all locations approximates the mean excess air volume, resulting in a better mixing effect compared to other cases. When fuel is ignited, rapid mixing of fuel and air leads to a quick rise in temperature. Subsequently, strong convection and radiation heat exchange cause the the flue gas temperature to decrease, and the residence time of the flue gas in the high-temperature zone shortens, resulting in a decrease in the amount of NO generated.

In conclusion, the factors influencing NO generation in the combustion chamber are not limited to combustion temperature and uniformity, but also involve mixing characteristics. The complex interaction of these factors makes the NO generation behavior in the combustion chamber more complex and variable.

4.2.4. Effect of air staging on incomplete combustion heat loss in the combustion chamber

Incomplete combustion in the combustion chamber indicates the quality of the combustion process, reflecting the degree of fuel burnout and overall combustion performance in heating furnaces.

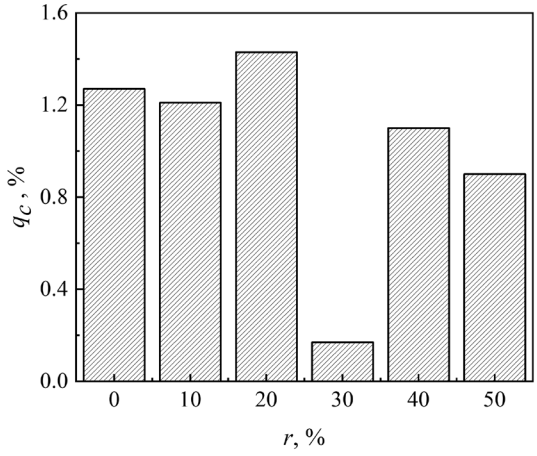

Fig. 11. Incomplete combustion heat loss q_c at different air staging ratios r.

The incomplete combustion heat loss q_c under various air staging ratios r was carefully calculated. As can be seen in Figure 11, when r = 30%, the heat loss of incomplete combustion is significantly lower compared to other supply air ratios, illustrating that with a primary-to-secondary air ratio of 7:3, fuel and air mix more thoroughly, resulting in a higher degree of complete combustion and enhanced combustion efficiency. The considerable heat loss of incomplete combustion observed under other operating conditions further implies that air staging influences the mixing and combustion of fuel and air, and the air staging ratio requires careful consideration.

5. Conclusions

Based on an existing top-fired heating furnace, a three-dimensional model of the combustion chamber was carefully constructed. The flow field, temperature distribution, and NO emission variations in the combustion chamber at different excess air coefficients were investigated. Additionally, the original primary air supply was changed for staged-air supply, altering the air staging ratio and its subsequent impact on the flow field, temperature profile, and NO emission levels in the combustion chamber when secondary air was introduced from the top of the heating furnace. The following conclusions were drawn.

1. The relationship between the excess air coefficient and the NO emission levels at the combustion chamber outlet does not show an obvious trend. As the excess air coefficient increases, NO emissions initially increase before decreasing. At an excess air coefficient of 1.05, the peak value is reached, after which the emission levels begin to decline.
2. Modifying the airflow mode and using air-staged combustion technology substantially affects the reduction of NO emission levels at the exit of the combustion chamber. Through simulation and analysis of various primary and secondary air ratios, an optimal ratio of 7:3 was identified. Under this ratio, the NO emission levels at the exit of the combustion chamber can be reduced to 36.90 mg/Nm^3, and the incomplete combustion heat loss of the fuel is lower compared to alternative ratios, indicating superior fuel combustion and greater combustion efficiency.
3. During air staging, the factors affecting the NO emission levels are complex and multifaceted. NO generation is influenced not only by combustion temperature and uniformity but also by mixing dynamics. The more uniform the mixing process, the lower the NO emission levels.

Acknowledgments

This work was financially supported by the Scientific Research Project of Education Department of Liaoning Province, China (grant No. L2020028).

We thank the reviewers for their careful reading of the manuscript and for providing valuable guidance and suggestions. The publication costs of this article were partially covered by the Estonian Academy of Sciences.

References

1. Liu, G., Sun, P., Ji, Y., Wan, Y., Wang, H., You, X. Current status and energy analysis of oil shale's retorting process in the world. *Pet. Chem.*, 2021, **61**(2), 123–138. http://dx.doi.org/10.1134/S0965544121020134
2. Xu, H., Zhao, Z., Bi, Z. Research on heating furnace technology of Fushun dry distillation technology. *Heilongjiang Sci. Technol. Inform.*, 2017, **1**(40), 40.
3. Wu, Q. *Oil Shale Distillation Technology*. Liaoning Science and Technology Press, Shenyang, 2012.
4. GB 31570-2015. Emission standard of pollutants for petroleum refining industry. Ministry of Ecology and Environment, China, 2015.
5. DB 37/2374-2018. Emission standard of air pollutants for boiler. Ministry of Ecology and Environment, China, 2018.
6. DB 11/139-2015. Beijing local standard boiler air pollutant emission standard. Beijing Municipal Environmental Protection Bureau, Beijing Municipal Bureau of Quality and Technical Supervision, China, 2015.
7. Vermot, A., Petit-Härtlein, I., Smith, S. M. E., Fieschi, F. NADPH oxidases (NO_x): an overview from discovery, molecular mechanisms to physiology and pathology. *Antioxidants*, 2021, **10**(6), 890.
8. Chen, X., Zhu, Y., Tao, J., Wang, C. NO_x emission performance and operation optimization of low nitrogen burner. *Chem. Ind. Eng. Prog.*, 2021, **40**, 1069–1076.
9. Wang, C., Wang, C., Pan, H., Yue, Y. Effect of structure parameters on low nitrogen performance of burner based on orthogonal experiment method. *Case Stud. Therm. Eng.*, 2022, **39**, 102404. https://doi.org/10.1016/j.csite.2022.102404
10. Zhu, Y., Wang, C., Chen, X. Combustion characteristic study with a flue gas internal and external double recirculation burner. *Chem. Eng. Process.: Process Intensif.*, 2021, **162**, 108345. http://dx.doi.org/10.1016/j.cep.2021.108345
11. Wang, Y., Li, X., Mao, T., Hu, P., Li, X., Wang, G. Mechanism modeling of optimal excess air coefficient for operating in coal fired boiler. *Energy*, 2022, **261**(A), 125128. https://doi.org/10.1016/j.energy.2022.125128
12. Pan, S. *Numerical Simulation of Low NO_x Gas Burners*. Master's thesis. Wuhan University of Science and Technology, China, 2021.
13. Liu, W., Ouyang, Z., Cao, X., Na, Y. The influence of air-stage method on flameless combustion of coal gasification fly ash with coal self-preheating technology. *Fuel*, 2019, **235**, 1368–1376. https://doi.org/10.1016/j.fuel.2018.08.127
14. Lin, J., Li, H., Zhang, Y., Yang, J. Experimental and numerical study of a two-stage swirl burner. *Energies*, 2022, **15**(3), 1097. http://dx.doi.org/10.3390/en15031097

15. Zhang, C. *Numerical Simulation Research of Tangential Bias Swirl Combustion*. Master's thesis. Shanghai Jiao Tong University, China, 2018.
16. Rashwan, S. S., Nemitallah, M. A., Habib, M. A. Review on premixed combustion technology: stability, emission control, applications, and numerical case study. *Energy Fuels*, 2016, **30**(12), 9981–10014. https://doi.org/10.1021/acs.energyfuels.6b02386
17. Han, J., Lou, G., Zhang, S., Wen, Z., Liu, X., Liu, J. The effects of coke parameters and circulating flue gas characteristics on NOx emission during flue gas recirculation sintering process. *Energies*, 2019, **12**(20), 3828. http://dx.doi.org/10.3390/en12203828
18. Wang, W., Liao, Y., Liu, J., Huang, Z., Tian, M. Numerical simulation and optimization of staged combustion and NO_x release characteristics in precalciner. *J. Therm. Sci.*, 2019, **28**(13), 1024–1034.
19. Li, Y., Lin, Y., Zhao, J., Liu, B., Wang, T., Wang, P., Mao, H. Control of NO_x emissions by air staging in small- and medium-scale biomass pellet boilers. *Environ. Sci. Pollut. Res.*, 2019, **26**(10), 9717–9729. https://link.springer.com/article/10.1007/s11356-019-04396-8
20. Ma, G. *Effects of Fushun Oil Shale Retorting Operation Factors Optimization*. Master's thesis. Jilin University, China, 2012.
21. Yue, Y., He, Z., Wang, C. H. Optimization of nozzle structure of top-burning heating furnace: case study of Fushun retort heating for oil shale. *Oil Shale*, 2024, **41**(2), 115–131. https://doi.org/10.3176/oil.2024.2.03
22. Zeng, Q. *Effect of Flue Gas Recirculation on NO_x Emissions Characteristics of Gas Non-Premixed Combustion*. Master's thesis. Chongqing University, China, 2018.
23. Tian, L. *Research and Optimization of Temperature Uniformity and Process Parameters of Roller Kiln*. Master's thesis. Guangdong University of Technology, China, 2020.